Published in final edited form as:
Cell. 2013 January 17; 152(1-2): 120–131. doi:10.1016/j.cell.2012.12.005.

Human TFIID binds to core promoter DNA in a reorganized structural state

Michael A. Cianfrocco[1], **George A. Kassavetis**[2], **Patricia Grob**[3], **Jie Fang**[3], **Tamar Juven-Gershon**[4], **James T. Kadonaga**[2], and **Eva Nogales**[3,5,6,*]

[1]Biophysics Graduate Group, University of California, Berkeley, CA 94720, USA

[2]Division of Biological Sciences, Section of Molecular Biology, University of California, San Diego, La Jolla, CA 92093-0347, USA

[3]Howard Hughes Medical Institute, University of California, Berkeley, CA 94720, USA

[4]Mina and Everard Goodman Faculty of Life Sciences, Bar-Ilan University, Ramat-Gan 52900, Israel

[5]Life Sciences Division, Lawrence Berkeley National Laboratory, Berkeley, CA 94720, USA

[6]Department of Molecular and Cell Biology, University of California, Berkeley, CA 94720, USA

Abstract

A mechanistic description of metazoan transcription is essential for understanding the molecular processes that govern cellular decisions. To provide structural insights into the DNA recognition step of transcription initiation, we used single particle electron microscopy to visualize human TFIID with promoter DNA. This analysis revealed that TFIID co-exists in two predominant and distinct structural states that differ by a 100Å translocation of TFIID's lobe A. The transition between these structural states is modulated by TFIIA, as the presence of TFIIA and promoter DNA facilitates the formation of a novel rearranged state of TFIID capable of promoter recognition and binding. DNA-labeling and footprinting, together with cryo-EM studies, mapped the locations of the TATA, Inr, MTE, and DPE promoter motifs within the TFIID-TFIIA-DNA structure. The existence of two structurally and functionally distinct forms of TFIID suggests that the different conformers may serve as specific targets for the action of regulatory factors.

INTRODUCTION

The regulation of gene expression is a complex task that is critical for the growth, development, and survival of organisms. Underlying its importance is the fact that while the number of protein coding genes has remained fairly constant throughout metazoan evolution, the number of regulatory DNA elements has increased dramatically (Levine and Tjian, 2003). By fine tuning both the rate and synchrony of transcription initiation by RNA polymerase II (RNAPII), transcriptional regulation can serve as a key control point to produce organism-wide changes in gene expression profiles in response to developmental and environmental cues (Levine, 2011).

*Corresponding author: ENogales@lbl.gov.

ACCESSION NUMBERS

Maps have been deposited in the Electron Microscopy Data Bank (EMDB) under accession numbers 10832 (TFIID-TFIIA-SCP rearranged), 10834 (TFIID-TFIIA-SCP canonical), 10835 (TFIID rearranged), and 10839 (TFIID canonical).

The initiation of transcription by RNAPII requires basal transcription factors known as TFIIA, TFIIB, TFIID, TFIIE, TFIIF, and TFIIH (Thomas and Chiang, 2006). These factors assemble onto the core promoters of protein coding genes to form a transcription pre-initiation complex (Buratowski et al., 1989; Rhee and Pugh, 2012). A sequential recruitment model has been proposed whereby TFIID and Mediator serve as coactivators that facilitate interactions between upstream and promoter proximal factors (Burley and Roeder, 1996). The interaction of TFIID with promoter DNA can be further stabilized through a TFIIA-mediated release of the inhibitory N-terminal domain of TAF1 from the concave DNA-binding surface of TATA binding protein (TBP) (Bagby et al., 2000; Geiger et al., 1996; Liu et al., 1998). The formation of the TFIID-TFIIA-DNA complex is then followed by the binding of TFIIB, RNAPII, TFIIF, TFIIE, and TFIIH to yield the transcriptionally competent pre-initiation complex (Thomas and Chiang, 2006).

TFIID is a multisubunit complex that comprises TBP and about 12 to 13 proteins termed TBP-associated factors (TAFs) (Burley and Roeder, 1996). Through the use of TBP and TAFs, TFIID makes sequence-specific contacts with core promoter DNA elements, including the TATA box, Initiator (Inr), motif ten element (MTE), downstream core promoter element (DPE), and downstream core element motifs (Juven-Gershon and Kadonaga, 2010). These interactions have been exploited to create a highly active core promoter, termed the “super core promoter” (SCP), which is capable of high affinity interactions with TFIID through the presence of optimal versions of the TATA, Inr, MTE, and DPE motifs (Juven-Gershon et al., 2006).

Despite the importance of TFIID as a coordinator of transcription initiation, high-resolution structural information has been restricted to crystal structures of a small number of subunits and domains within TFIID (Bhattacharya et al., 2007; Jacobson et al., 2000; Kim et al., 1993a; Kim et al., 1993b; Liu et al., 1998; Werten et al., 2002; Xie et al., 1996). The size and scarcity of TFIID, typically purified from endogenous sources, has restricted structural studies to methods requiring microgram quantities of sample. Single-particle electron microscopy (EM) has proven to be an indispensable tool for the structural characterization of large multisubunit complexes, even when sample is available in minute amounts. This technique also has the potential to characterize the structural dynamics of large protein complexes (Leschziner and Nogales, 2007).

EM structural studies of TFIID have yielded low-resolution structures (20 to 30 Å) of yeast and human TFIID (Andel et al., 1999; Brand et al., 1999; Elmlund et al., 2009; Grob et al., 2006; Leurent et al., 2002; Leurent et al., 2004; Liu et al., 2009; Papai et al., 2010; Papai et al., 2009). A number of these studies suggested a role of conformational flexibility in promoter binding by TFIID. Recently, several groups have reported single particle EM structures of purified endogenous yeast TFIID bound to promoter DNA. These studies examined the binding of TFIID from *Schizosaccharomyces pombe* and *Saccharomyces cerevisiae* to promoters that contain both TATA and Inr sequence elements (Elmlund et al., 2009; Papai et al., 2010). Computational methods were used to sort TFIID into distinct conformational states, and additional densities, which were attributed to TATA box DNA, were localized to the surfaces of their structures.

To gain insight into the function of metazoan TFIID, we have applied single particle EM and extensive image sorting methodologies to characterize the structural dynamics of human TFIID. We found that TFIID exhibits a surprising degree of flexibility, moving its lobe A (~ 300 kDa in size) by 100 Å across the central channel of TFIID in a dynamic equilibrium. These findings revealed a novel “rearranged” conformation of TFIID that corresponds to a high affinity DNA binding state. By using gold labeling and multi-model refinements, we have defined the organization of the rearranged conformation of TFIID bound to promoter

DNA. The protein-DNA interactions were further probed by carrying out DNA footprinting experiments with DNase I and methidiumpropyl-EDTA-Fe(II), and the digestion patterns on wild-type and mutant SCP were mapped onto the cryo-EM structure of TFIID-TFIIA-SCP. These studies suggest a model in which the distinct conformations of TFIID may serve as targets through which regulatory factors recruit TFIID to specific types of core promoters.

RESULTS

Lobe A is flexibly attached to a stable core of TFIID that comprises lobes B and C

In a previous cryo-EM analysis of human TFIID, the use of a 3D variance approach indicated that conformational flexibility is an intrinsic property of TFIID (Grob et al., 2006). Due to the potential role of this flexibility in TFIID function, we investigated this property more thoroughly by extensive 2D image analysis of negatively stained TFIID samples. By concentrating specifically on a “standard” view, where the three main lobes of TFIID – lobes A, B and C – are clearly separated and distinguishable, we were surprised to find that lobe A was present in a range of positions with respect to a more stable core of the complex formed by lobes B and C (termed the “BC core”) (Figure S1A). This dramatic movement of lobe A represented a structural reorganization of TFIID that was not fully appreciated in the previous work on human TFIID.

We further examined these substantial differences in the positioning of lobe A within TFIID. Subclassification within a 2D mask that excluded the stable BC core revealed that lobe A adopts a wide range of positions (Figures S1B & C). This analysis recovered a previously described structure in which lobe A is located near lobe C, and we will refer to this arrangement as the “canonical” state of human TFIID (Andel et al., 1999; Grob et al., 2006; Liu et al., 2008; Liu et al., 2009). In addition, we found that lobe A can also be positioned across the TFIID central channel at a new location in which it contacts lobe B (Figure S1C). In this conformation, TFIID forms a “rearranged” horseshoe-like structure wherein the order of the lobes has been altered. We refer to this conformation as the “rearranged” state (Figure S1C). To rule out that these distinct positions of lobe A were an artifact due to the negative staining procedures, we carried out an identical analysis using cryo-EM images of the same TFIID sample (Figure S1D). A similar range of positions of lobe A with respect to a stable BC core was detected in the frozen-hydrated TFIID sample, thus confirming the coexistence of these distinct states of the complex (Figure 1, Supplemental Movie 1).

To quantify the structural plasticity exhibited by TFIID, the position of lobe A along the BC core was measured within each sub-classified average. The measurements were normalized so that values greater than 0.70 correspond to particles resembling the canonical state, in which lobe A is at its closest position to lobe C (Figure S1E). Values less than 0.50, on the other hand, indicate that the particles are in a rearranged state, wherein lobe A is proximal to lobe B (Figure S1E). This analysis revealed that the position of lobe A can be described by a bi-modal distribution with peaks centered at 0.40 and 0.80 (Figure 2A). Surprisingly, this analysis showed that approximately 50% of the TFIID particles are found in the rearranged state. These distinct structural states of TFIID were observed in datasets from both cryo-EM and negative stain data, demonstrating that the sample preparation did not alter the results (Figure S1F). Hence, there are two predominant and structurally distinct states of TFIID that differ the reorganization of lobe A within the complex.

The conformational landscape of TFIID is affected by TFIIA and promoter DNA

To examine whether the binding of TFIIA and promoter DNA is linked to the conformational states of TFIID, we analyzed TFIID in the presence of excess super core promoter (SCP) DNA and/or the cofactor TFIIA. The SCP contains the TATA box, Inr,

MTE, and DPE core promoter motifs. When TFIID was incubated with SCP DNA and negatively stained samples were visualized and analyzed as described above, lobe A showed a similar distribution of positions relative to TFIID (Figure 2B) ($p = 0.0353$, Wilcoxon signed-rank test). This result suggested either that TFIID does not interact with SCP under the conditions used, or that DNA binding does not alter the conformational partitioning of lobe A within the accuracy of our measurements.

We then tested whether the presence of TFIIA affects the properties of TFIID. When TFIID was incubated with TFIIA in the absence of DNA, the distribution of lobe A positions was shifted to the peak centered at 0.80. It thus appears that TFIIA stabilizes TFIID in the canonical state (Figure 2C). On the other hand, in the presence of SCP DNA, TFIIA promotes the formation of the rearranged state of TFIID, with a strong increase in the peak of lobe A positions centered at 0.40 (Figure 2D). The distribution of lobe A positions within the context of TFIID-TFIIA (Figure 2C) was significantly different from that seen with TFIID-TFIIA-SCP (Figure 2D) ($p = 1.5 \times 10^{-13}$, Wilcoxon signed-rank test). Since TFIID is purified using established protocols (Liu et al., 2008; Liu et al., 2009), any underlying biochemical heterogeneity will be constant between these experiments, suggesting that these conformational changes are due to the presence of TFIIA and SCP DNA. These results indicate that TFIIA serves the dual function of maintaining TFIID in the canonical state in the absence of DNA and promoting the formation of the rearranged state in the presence of promoter DNA.

The rearranged state of TFIID binds SCP DNA in the presence of TFIIA

To characterize the structure of this novel rearranged state of TFIID and its binding to DNA, we carried out cryo-EM visualization of frozen hydrated samples. Analysis of 2D reference-free averages from cryo-EM data of the TFIID-TFIIA-SCP ternary complex showed the presence of both the rearranged and canonical states (Figures 3A & B, leftmost panels). Importantly, the class averages corresponding to the rearranged state revealed extra density that appeared to be DNA extending across the central channel of TFIID (Figure 3A, left panel). This additional density was confirmed to be DNA by examining cryo-EM 2D reference-free class averages collected for TFIID, TFIID-SCP, and TFIID-TFIIA. 2D reference-free class averages of TFIID without the combined presence of TFIIA and SCP showed no extra density within the rearranged state (Figure 3A). These observations suggest that TFIIA is required for efficient binding of TFIID to SCP and that the predominant form of TFIID that is bound to DNA is the novel rearranged state.

Cryo-EM structures of the rearranged and canonical states of TFIID

The 2D image analysis indicated that both TFIID and the ternary TFIID-TFIIA-SCP samples exist in a distribution of conformational states (Figures 2A & D), and thus, cryo-EM reconstructions of these samples needed to involve a multi-model 3D refinement strategy. A total of ~35,000 cryo-EM particle images from the purified TFIID-TFIIA-SCP complex were sorted using multi-reference projection matching with two distinct *ab initio* references structures that were obtained using the orthogonal tilt reconstruction method (Leschziner and Nogales, 2006) (Figure S2, and Extended Experimental Procedures) and that represent the rearranged and canonical conformations. After implementing a cross-correlation cutoff that excluded 25% of the particles, the reconstruction of the rearranged state (comprising ~ 60% of the remaining particles) was refined to a resolution of 32 Å (Figures 3C, S3B – D). A prominent feature of the rearranged structure is the presence of density (green, Figure 3C), which we attribute to DNA, extending over lobe C and across the central channel of TFIID towards the region connecting lobes A and B. Although the DNA density exhibits one location of weak connectivity at the standard threshold for the

molecular weight of TFIID-TFIIA-SCP (~1.2 MDa), a continuous density can be observed across the central cavity of TFIID at a slightly lower threshold (Figure S3A).

A 3D model for the canonical state was refined simultaneously from the TFIID-TFIIA-SCP samples to a similar resolution and included the remaining 40% of the selected particles (Figures 3E, S3B – D). Importantly, the canonical state does not show the presence of any apparent DNA density, but is otherwise similar in overall features to the previously reported cryo-EM (Grob et al., 2006) and negative stain (Liu et al., 2009) structures of human TFIID. Comparison of the coexisting canonical and rearranged structures confirms the presence of a common BC core (blue, Figures 3C & E). However, the position of lobe A is dramatically shifted from one side of the core to the other, where lobe A is within close proximity of the DNA binding site of lobe C (yellow, Figure 3C; orange, Figure 3E). The movement of lobe A from the canonical state to the rearranged state involves a translational component along the BC core axis (Supplementary Movie 2), as lobe A changes its apparent connectivity from lobe C (canonical) to lobe B (rearranged). These two reconstructions from the TFIID-TFIIA-SCP sample suggest that TFIID exhibits high affinity DNA interactions only when it adopts the rearranged conformation, considering the lack of any apparent DNA density for the canonical conformation.

The assignment of DNA as the narrow, linear density present only in the rearranged state of the TFIID-TFIIA-SCP sample was further supported by comparison of the cryo-EM structure of the rearranged state with that of the TFIID sample. Using the same multi-model approach described above, we obtained 3D cryo-EM reconstructions of the two alternative states of TFIID (Figures 3D & F, S3F – H). Comparison of the rearranged conformation (~50% of selected particles) of TFIID with the structure of TFIID-TFIIA-SCP shows that there is strong density, which we ascribe to DNA, that is uniquely in the ternary complex and extends across the TFIID channel from lobe C to lobe A (Figures 3C & D, S3A & E). The structures of the canonical conformation of TFIID observed with TFIID alone and with the TFIID-TFIIA-SCP sample appear to be similar (Figures 3E & F, Supplementary Movie 2), which suggests that the particles in the canonical conformation in the TFIID-TFIIA-SCP sample lack stably positioned SCP DNA.

Promoter DNA path through TFIID

We then examined the orientation of the DNA bound to the rearranged TFIID-TFIIA-SCP complex. First, cryo-EM data were collected from a sample of TFIID, TFIIA, and SCP DNA with a 30 bp 5′ extension to position −66 (termed "−66") upstream of the TATA box (Figure 4A). Comparison of cryo-EM 3D reconstructions for the rearranged state of TFIID-TFIIA-SCP(−66) and TFIID-TFIIA-SCP revealed significant extra density extending out of lobe A, which was the strongest difference between the two cryo-EM reconstructions at σ = 4 (Figure 4A, arrows, Supplementary Movie 2). The dimensions of this additional density are consistent with the length of the DNA extension (Figure 4A, right). Beyond identifying the upstream DNA sequence at position −66, this additional DNA density extending from lobe A also provided a marker for the position of the TATA box, which is 36 bp from the end of this extended DNA, and thus within lobe A of the rearranged state (Figure 4A).

We further examined the orientation of promoter DNA on TFIID by covalent labeling of the SCP DNA with 1.4 nm maleimido-Nanogold at either −36 (TATA box) or +45 on the SCP promoter sequence. This strategy takes advantage of the high contrast of Nanogold relative to that of protein and DNA in transmission EM, providing a strong signal for the localization of gold particles relative to protein and DNA density (see Extended Experimental Procedures). Analysis of the 2D reference-free class averages for TFIID-TFIIA-SCP(+45 gold) revealed that the downstream region of the SCP is bound by lobe C (Figure 4B). Moreover, consistent with our DNA extension experiment, Nanogold labeling of TFIID-

TFIIA-SCP(TATA gold) demonstrated that the upstream DNA sequence is bound by TFIID within lobe A at a location across the central channel from lobe C (Figure 4C).

TFIIA localizes to lobe A in both the canonical and rearranged conformations of TFIID

We next investigated the location of TFIIA in the rearranged TFIID-TFIIA-SCP complex by analysis of TFIIA that was labeled with 1.8 nm Ni^{2+}-NTA-Nanogold. Upon 2D reference-free analysis of the high defocus cryo-EM particles, the determined alignment parameters were applied to the low defocus focal mate and class averages were calculated. Nanogold densities identified the TFIIA binding site within lobe A of the rearranged state (Figure 4D), adjacent to the TATA Nanogold location (Figure 4C). Importantly, analysis of 2D reference-free class averages corresponding to the canonical state also demonstrated that TFIIA localized to lobe A in its alternate configuration relative to the BC core (Figure 4E). These findings are in agreement with the well-characterized direct interaction of TBP and TFIIA, and further demonstrate, in the context of TFIID, that TFIIA interacts with the complex at a location close to the TATA box-binding site. These findings therefore suggest that both TBP and TFIIA are localized within lobe A during the structural transition between canonical and rearranged states of TFIID.

Footprinting analyses of TFIID-promoter contacts in the presence or absence of TFIIA

The cryo-EM data of the rearranged conformation of the TFIID-TFIIA-SCP complex suggest that the downstream DNA core promoter elements MTE and DPE are bound by lobe C, whereas the TATA box and possibly the Inr are bound by lobe A. To test and extend this model, we performed footprinting analyses of the TFIID-SCP complex in the presence or absence of TFIIA.

DNase I footprinting of TFIID-SCP showed an extended region of protection from −7 to +41, which is in agreement with previous footprinting data on TFIID-SCP (Figure 5A) (Juven-Gershon et al., 2006). The addition of TFIIA did not alter the downstream interactions of TFIID with the Inr, MTE, and DPE core promoter elements, but did, however, result in a substantial increase in the binding of TFIID to the TATA box and flanking DNA sequences from −38 to −20 (Figures 5A, S4A & B). DNase I footprinting analysis of both DNA strands in the absence or presence of TFIIA revealed distinct patterns of protection and cleavage throughout the core promoter region. The results indicate that the DNA sequence between the Inr and MTE/DPE sites exhibits a phasing in DNase I sensitivity in which one face of the SCP DNA between Inr and MTE-DPE is susceptible to DNase I cleavage, whereas the opposite face remains protected (Figure 6). Furthermore, the accessible face of the DNA exhibits DNase I hypersensitivity upon binding of TFIID (Figure 5A).

To obtain high resolution data on the interactions of TFIID with the core promoter, we carried out footprinting analyses with methidiumpropyl-EDTA-Fe(II) (MPE-Fe), an intercalating agent that delivers Fe(II) for oxidation of the deoxyribose phosphate backbone of DNA and provides single bp resolution of protein-DNA contacts (Hertzberg and Dervan, 1984; Papavassiliou, 1995; Van Dyke et al., 1982). The MPE-Fe footprinting data on TFIID-SCP and TFIID-TFIIA-SCP revealed the extensive and continuous interaction of TFIID with DNA from the DPE through the Inr as well as the TFIIA-dependent protection of 8 bp (−31 to −24) of DNA encompassing the TATA box (Figures 5B, S4C & D). The strong stimulation of TFIID binding to the TATA box is consistent with the results of previous studies on the binding of TBP to DNA (Geiger et al., 1996; Kim et al., 1993a; Kim et al., 1993b; Nikolov et al., 1995). The region of DNase I protection observed on only one face of the helix between the MTE/DPE and Inr also shows continuous protection from MPE-Fe(II) cleavage on both DNA strands, which is likely due to the inhibition of the DNA unwinding,

necessary for MPE intercalation, that would occur as a result of protein bound to one side of the helix (Uchida et al., 1989). Thus, the DNase I and MPE-Fe footprinting results, summarized in Figure 6A & B and Supplementary Movie 2, provide insight into the TFIID-DNA contacts that complements the cryo-EM data and contributes to the placement of the core promoter DNA on the TFIID structure.

To explore the effect of core promoter architecture on TFIID-promoter interactions, DNase I footprinting experiments were performed with 'mutant' SCP DNA constructs in the presence or absence of TFIIA (Figure 5C). Mutation of the TATA box within the SCP sequence (mTATA) resulted in a wild-type interaction with the promoter DNA from the Inr to the DPE, as seen previously (Juven-Gershon et al., 2006). In addition, the inclusion of TFIIA resulted in a weak but detectable footprint over the mutant TATA box (Figure S5). The strong resemblance between the mTATA and the wild-type SCP DNase I protection patterns suggested that TFIID is bound to the mTATA sequence in the rearranged conformation. To test this hypothesis, we collected cryo-EM data and visualized a sample of TFIID-TFIIA-SCP(mTATA) (Figure S6). This experiment revealed that TFIID binds to the mTATA promoter in a nearly identical conformation as that observed with the wild-type SCP sequence. Thus, the combined footprinting and EM data indicate that the rearranged state of TFIID serves as the predominant DNA binding conformation for the SCP and mTATA promoter architectures.

The conformation of promoter-bound TFIID was further addressed by analysis of promoters that contain mutations in the Inr (mInr) or MTE/DPE (mMTE/DPE) promoter motifs (Figure 5C). TFIID did not interact appreciably with either the mInr promoter or the mMTE/DPE promoter in the absence of TFIIA, as seen previously (Juven-Gershon et al., 2006). However, the addition of TFIIA resulted in strong binding of TFIID to the TATA box as well as to sequences from the Inr through the DPE regions. In the presence of TFIIA, the overall patterns of protection observed with the mInr and mMTE/DPE promoters are similar to those seen with the wild-type SCP. It thus appears likely that TFIID-TFIIA binds to the mInr and mMTE/DPE promoters in the rearranged conformation. Hence, the footprinting and EM data both suggest that TFIID binds to the wild-type and mutant SCPs in the newly discovered rearranged conformation.

DISCUSSION

Promoter-bound TFIID is in a novel rearranged conformation

We have applied single particle EM analysis to describe a dynamic conformational landscape for human TFIID. The TFIID complex exists in a canonical state, in which lobe A interacts with lobe C, as well as a rearranged state, in which lobe A is found in a reorganized position bound to lobe B. Most notably, the rearranged state of TFIID appears to be the form of TFIID that is bound to core promoter DNA, whereas the canonical state of TFIID appears to be the form of free TFIID. EM-based mapping, together with footprinting experiments on promoter DNA, have allowed us to define the approximate locations of the core promoter elements as well as the TFIIA cofactor on the rearranged form of TFIID. The architecture of the rearranged conformation of TFIID may be an important component in the assembly of the pre-initiation complex.

Our visualization of the rearranged TFIID-TFIIA-SCP complex provides the first structural insight into a previously proposed 'isomerization' of human TFIID (Chi and Carey, 1996; Emami et al., 1997; Lieberman and Berk, 1994). These and other studies have probed TFIIA- and activator-dependent interactions between human TFIID and downstream promoter regions, where downstream DNA contacts developed only after TFIID was recruited to the promoter through TBP-TATA interactions. From this observation, TFIID

was proposed to undergo an ‘isomerization’ as it created TAF-DNA contacts away from the original site of interaction at the TATA box. While the authors did not have any information on the structure of TFIID at that time, we can now explain their biochemical footprinting data given the interplay between TFIID’s structural dynamics and promoter binding that we observed in our cryo-EM experiments. This is an example of how our structural analysis can provide fundamental mechanistic insight and serve as a framework to describe decades of biochemical experimentation with human TFIID.

We believe that our ability to map the extensive interactions between human TFIID and promoter DNA goes well beyond previously published work concerning the binding of yeast TFIID to DNA (Elmlund et al., 2009; Papai et al., 2010). When probed with DNase I footprinting (Sanders et al., 2002), yeast TFIID only makes TATA box contacts (< 10 bps). Perhaps because of this small contact region, EM studies of yeast TFIID were unable to localize clearly the promoter DNA bound to their structure. In contrast, our work with human TFIID and the SCP allowed us to visualize unambiguously large and continuous densities for promoter DNA: 50 bps across the central channel of TFIID from lobe C to lobe A and 20 bps of upstream exiting lobe A. Our direct observation of DNA bound by human TFIID, in combination with our gold labeling and footprinting studies, provides a detailed structural model for TFIID’s 100 bp footprint on promoter DNA. We speculate that the accessibility of DNA segments near the TSS within the rearranged conformation of TFIID provides a model of promoter-bound TFIID that may be primed for RNAPII loading at the transcription start site.

It is possible that the structural dynamics of lobe A described here may be present in all eukaryotic forms of TFIID. The structural differences observed between previous 3D models of yeast and human TFIID (Papai et al., 2011) may be, at least in part, due to the structural plasticity of the TFIID complex. While it is still possible that these structural differences may reflect true divergence between species, we believe that the conformational changes seen in this study may need to be considered within the context of previous biochemical and structural data on yeast and human TFIID (Andel et al., 1999; Elmlund et al., 2009; Grob et al., 2006; Leurent et al., 2002; Leurent et al., 2004; Liu et al., 2008; Liu et al., 2009; Papai et al., 2010).

The extremely flexible attachment of lobe A within TFIID posed a significant challenge in the determination of the structure of human TFIID bound to promoter DNA (Figures 3 & 4). The underlying structural transitions explain why our earlier attempts to obtain a 3D reconstruction of TFIID-TFIIA-SCP using a single canonical model were unable to provide a stable 3D structure (data not shown). It was only after re-derivation of two distinct starting models using *ab initio* single particle EM methods that 3D models were described corresponding to both the canonical and rearranged conformations, with the latter corresponding to the DNA-bound form of the complex. Even after taking these two predominant conformations into account, the resolution of the structures is limited by the flexibility of lobe A within TFIID present in both conformations (Figure 2). This flexibility, combined with the presence of stabilizing agents (detergent, sugar, and glycerol) within the sample buffer and the use of a carbon film as support, both of which decrease the contrast of the images, has so far prevented the accurate particle alignments necessary for high-resolution refinement of the data. The advent of technical developments that will ultimately improve the signal-to-noise-ratios in cryo-EM images (e.g. direct electron detection, phase plate implementations) hold the promise for obtaining the contrast necessary to partition TFIID into specific conformations in order to achieve higher resolution.

The interaction of human TFIID with promoter DNA

Lobe C interacts with downstream promoter DNA elements—We have developed a model to describe the DNA path through the modular subdomains of the TFIID-TFIIA-SCP complex (Figures 6A & B, Supplementary Movie 2). Gold labeling of the SCP DNA at the +45 position indicated that the density extending off of lobe C is the downstream promoter DNA (Figure 4B). It thus appears that the MTE and DPE promoter elements are bound by lobe C (Figures 6A & B), which suggests that lobe C contains subunits TAF6 and TAF9 (Burke and Kadonaga, 1997; Theisen et al., 2010). The presence of DNA on the surface of lobe C is consistent with the DNase I footprinting data, which revealed that one face of the downstream promoter DNA is protected whereas the other face is exposed to solution and accessible for cleavage by DNase I (6A & B, middle). On each strand between the Inr and MTE, there is a distinct 10 bp phasing of DNase I hypersensitive sites at −2, +18, and +28 (with probe DNA 5′-labeled upstream) and at +4 and +13 (with probe DNA 5′-labeled downstream). This periodic DNase I digestion pattern is consistent with the promoter DNA being rotationally positioned on the surface of TFIID.

Lobe A contacts promoter DNA upstream of the TSS—Across the central channel from lobe C, the flexibly attached lobe A interacts with SCP DNA extending from the Inr to the TATA box (Figures 6A & B). Previous work demonstrated that this region of the core promoter interacts with a TAF1, TAF2, and TBP subcomplex that is also able to direct transcription from TATA-Inr promoters (Chalkley and Verrijzer, 1999). Given the modularity of lobe A within the context of TFIID, it is likely that lobe A contains TAF1, TAF2, and TBP and serves as a modular domain of TFIID that is capable of interactions with promoter DNA upstream of the TSS.

This proposed composition of lobe A is consistent with studies addressing the integrity of the TFIID complex *in vivo* (Wright et al., 2006). Through systematic RNAi-mediated knockdown, the authors defined a stable TAF4, −5, −6, −9 and −12 subcomplex nucleated by TAF4. In contrast, knockdown of TAF1, TAF2, TAF11, or TBP did not affect the integrity of the TFIID complex, suggesting a peripheral location within TFIID. Thus, lobe A likely comprises TAF1, TAF2, TAF11, and TBP, existing as a modular domain of TFIID, whereas a stable TAF4, −5, −6, −9 and −12 subcomplex may correspond to the BC core.

To model the DNA path through lobe A, two bends within lobe A were incorporated to accommodate the 120° angle that TFIID imposes on the downstream and upstream DNA regions (Figure 6B). Initial attempts to trace the DNA path through the TFIID-TFIIA-SCP structure using a single bend at the TATA box failed to generate a model that was compatible with the experimentally obtained positions of downstream and upstream DNA locations (data not shown). Given the angle of upstream DNA and the location of the −66 position, we modeled the location of TBP and TATA box DNA to be 36 bp (12.2 nm) downstream from the −66 position observed in the TFIID-TFIIA-SCP(−66) structure. After incorporating this bend at −31/30, a second gradual bend is proposed to form along the DNA between the TATA box and Inr. We suggest that this DNA deformation between the TATA box and Inr could play a role in positioning TBP and TFIIB in close proximity to the TSS for efficient loading of RNAPII.

TFIID interacts with diverse promoter architectures through the rearranged conformation

Because the majority of promoters within the *Drosophila* and human genomes do not contain all four of the core promoter motifs engineered into the SCP (Juven-Gershon and Kadonaga, 2010), we analyzed promoter architectures with fewer core promoter motifs to investigate the relevance of the rearranged TFIID-TFIIA-SCP structure. To this end, we compared TFIID interactions with ‘wild-type’ versus ‘mutant’ versions of the SCP (Figure

5C). These data suggest that TFIID interacts with TATA-Inr, TATA-MTE/DPE, and Inr-MTE/DPE promoters in the newly described rearranged conformation.

With the 'wild-type' SCP as well as with the three 'mutant' (mTATA, mInr, mMTE/DPE) versions of the SCP, we observed that TFIIA stimulates the binding of TFIID to the TATA box region (Figure 5C). This effect is consistent with the well-established TFIIA-mediated enhancement of TBP binding to the TATA box (Thomas and Chiang, 2006). With the mTATA promoter, the primary interaction of TFIID with the DNA is via the Inr, MTE, and DPE motifs, and a weak stimulation by TFIIA of the binding of TFIID to the mutant TATA box region is also observed. With the mInr and mMTE/DPE promoters, it seems likely that TFIIA stimulates the binding of TBP to the TATA box and that the remainder of the TFIID complex then interacts with the Inr through the DPE region of the core promoter, irrespective of the presence of consensus Inr or MTE/DPE elements. These findings may be analogous to the previously observed stimulation of the binding of partially-purified TFIID to the downstream promoter region of the adenovirus major late promoter (which lacks MTE/DPE motifs) by the upstream stimulatory factor, USF (Sawadogo and Roeder, 1985; Van Dyke et al., 1988). In this light, it is possible that other sequence-specific activators, as well as coactivators, may function in a related manner to stabilize TFIID on promoter DNA and thus promote the formation of the rearranged conformation.

We believe that our description of the conformational landscape of TFIID presents a conceptual framework for understanding the functional interactions between TFIIA and core promoter architecture on TFIID structure. In particular, the dynamic conformational landscape of TFIID may have regulatory consequences within the cell by providing specific structural targets that can be recognized by transcriptional activators and repressors.

EXPERIMENTAL PROCEDURES

Full details of experimental procedures are presented in the Extended Experimental Procedures.

Protein and Nucleic Acid Preparation

Purification of human TFIID and TFIID-TFIIA-SCP was performed as described previously (Grob et al., 2006; Liu et al., 2009). Briefly, fractionated Hela nuclear extract was subjected to immunoprecipitation with a α-TAF4 monoclonal antibody (BD Biosciences). Assembly of the TFIID-TFIIA-SCP complex involved adding a 10X-excess of recombinant TFIIA (Sun et al., 1994) and SCP DNA (IDT) prior to elution from the resin (Figure S7).

The DNA sequence used for the SCP was taken directly from the originally published sequence of SCP1 (Juven-Gershon et al., 2006):

GTACTTATATAAGGGGGTGGGGGCGCGTTCGTCCTCAGTCGCGATCGAACA
CTCGAGCCGAGCAGACGTGCCTACGGACCG

For SCP(−66), the following sequence was added immediately upstream of the SCP sequence:

CTCGCGCCACCTCTGTTTTCCCAGTCACGA

Mutant promoter sequences were taken directly from previous mutational analysis of SCP1 (Juven-Gershon et al., 2006).

Sample preparation & EM

For negative stain microscopy, four microliters of TFIID sample was directly applied to glow discharged holey carbon film covered with a continuous thin-carbon support on a 400

mesh copper grid (Electron Microscopy Sciences). For cryo-EM, samples were vitrified using a Vitrobot (Gatan, Inc.) that was set to 100% humidity at 4°C. Four microliters of sample was incubated for 30 sec. −1 min. on carbon-thickened C-flat grid (Protochips) with 4 μm holes that were spaced 2 μm apart that had a thin-carbon support within the holes, blotted for 6.5 s, and then plunge-frozen in liquid ethane.

Negative stain data shown in Figure 2 were collected using a Tecnai T12 bio-TWIN transmission EM operating at 120 keV under low dose (15 $e^{-}/Å^2$) conditions on Kodak SO163 film at a nominal magnification of 30,000X from defocuses ranging from −0.70 μm to −1.20 μm. Micrographs were digitized in a Nikon Super Coolscan 8000 at a pixel size of 12.7 μm (4.23 A/pix). Cryo-EM data were collected on a Tecnai F20 TWIN transmission EM operating at 120 keV using a dose of 25 $e^{-}/Å^2$ on a Gatan 4k × 4k CCD at a nominal magnification of 80,000X (1.501 Å/pixel). Leginon software was used to automatically focus and collect exposure images (Suloway et al., 2005).

Image preparation & analysis

Particles from the negative stain data shown in Figure 2 were manually picked using Boxer (EMAN) (Ludtke et al., 1999), CTF-estimated using CTFFIND3 (Mindell and Grigorieff, 2003), and phase-flipped using SPIDER (Frank et al., 1996). Cryo-EM data were prepared using the Appion image processing environment (Lander et al., 2009) where particles were automatically picked using Signature (Chen and Grigorieff, 2007), CTF-estimated using CTFFIND3 (Mindell and Grigorieff, 2003), phase flipped using SPIDER (Frank et al., 1996), and normalized using XMIPP (Sorzano et al., 2004).

For negative stain, 2D reference-free image analysis was performed using an iterative routine implementing a topology representing network (Ogura et al., 2003) in combination with mutli-reference-alignment within IMAGIC (van Heel et al., 1996). For cryo-EM, 2D reference-free image analysis was performed exclusively within IMAGIC (van Heel et al., 1996) through iterative rounds of multivariate statistical analysis and multi-reference-alignment.

3D refinements were performed on phase-flipped particles using an iterative projection matching and 3D reconstruction approach that was performed using libraries from EMAN2 and SPARX software packages (Hohn et al., 2007; Tang et al., 2007). 34,167 particles from cryo-EM grids prepared from TFIID-TFIIA-SCP sample were refined against low-pass filtered models of the canonical and rearranged state. For TFIID, 30,800 particles were collected and refined. Following this global projection matching routine, all data were further refined in FREALIGN (Grigorieff, 2007) and low-pass filtered at the final resolution while applying a negative B-factor using *bfactor.exe*.

Supplementary Material

Refer to Web version on PubMed Central for supplementary material.

Acknowledgments

We thank members of the Nogales lab for constant advice and help with EM analysis; R. J. Hall for initial work on this project; A. Leschziner for advice on the implementation of OTR; S. Zheng for providing TAF4 mAb; D. King for peptides; R. Tjian, W.L. Liu, and R. Coleman for critical feedback and helpful discussions. This work was supported by grants from the National Institutes of Health (GM041249 to J.T.K., GM63072 to E.N.). E.N. is a Howard Hughes Medical Institute Investigator.

References

Andel F 3rd, Ladurner AG, Inouye C, Tjian R, Nogales E. Three-dimensional structure of the human TFIID-IIA-IIB complex. Science. 1999; 286:2153–2156. [PubMed: 10591646]

Bagby S, Mal TK, Liu D, Raddatz E, Nakatani Y, Ikura M. TFIIA-TAF regulatory interplay: NMR evidence for overlapping binding sites on TBP. FEBS Lett. 2000; 468:149–154. [PubMed: 10692576]

Bhattacharya S, Takada S, Jacobson RH. Structural analysis and dimerization potential of the human TAF5 subunit of TFIID. Proc Natl Acad Sci U S A. 2007; 104:1189–1194. [PubMed: 17227857]

Brand M, Leurent C, Mallouh V, Tora L, Schultz P. Three-dimensional structures of the TAFII-containing complexes TFIID and TFTC. Science. 1999; 286:2151–2153. [PubMed: 10591645]

Buratowski S, Hahn S, Guarente L, Sharp PA. Five intermediate complexes in transcription initiation by RNA polymerase II. Cell. 1989; 56:549–561. [PubMed: 2917366]

Burke TW, Kadonaga JT. The downstream core promoter element, DPE, is conserved from Drosophila to humans and is recognized by TAFII60 of Drosophila. Genes Dev. 1997; 11:3020–3031. [PubMed: 9367984]

Burley SK, Roeder RG. Biochemistry and structural biology of transcription factor IID (TFIID). Annu Rev Biochem. 1996; 65:769–799. [PubMed: 8811195]

Chalkley GE, Verrijzer CP. DNA binding site selection by RNA polymerase II TAFs: a TAF(II)250-TAF(II)150 complex recognizes the initiator. EMBO J. 1999; 18:4835–4845. [PubMed: 10469661]

Chen JZ, Grigorieff N. SIGNATURE: a single-particle selection system for molecular electron microscopy. J Struct Biol. 2007; 157:168–173. [PubMed: 16870473]

Chi T, Carey M. Assembly of the isomerized TFIIA--TFIID--TATA ternary complex is necessary and sufficient for gene activation. Genes Dev. 1996; 10:2540–2550. [PubMed: 8895656]

Elmlund H, Baraznenok V, Linder T, Szilagyi Z, Rofougaran R, Hofer A, Hebert H, Lindahl M, Gustafsson CM. Cryo-EM reveals promoter DNA binding and conformational flexibility of the general transcription factor TFIID. Structure. 2009; 17:1442–1452. [PubMed: 19913479]

Emami KH, Jain A, Smale ST. Mechanism of synergy between TATA and initiator: synergistic binding of TFIID following a putative TFIIA-induced isomerization. Genes Dev. 1997; 11:3007–3019. [PubMed: 9367983]

Frank J, Radermacher M, Penczek P, Zhu J, Li Y, Ladjadj M, Leith A. SPIDER and WEB: processing and visualization of images in 3D electron microscopy and related fields. J Struct Biol. 1996; 116:190–199. [PubMed: 8742743]

Geiger JH, Hahn S, Lee S, Sigler PB. Crystal structure of the yeast TFIIA/TBP/DNA complex. Science. 1996; 272:830–836. [PubMed: 8629014]

Grigorieff N. FREALIGN: high-resolution refinement of single particle structures. J Struct Biol. 2007; 157:117–125. [PubMed: 16828314]

Grob P, Cruse MJ, Inouye C, Peris M, Penczek PA, Tjian R, Nogales E. Cryo-electron microscopy studies of human TFIID: conformational breathing in the integration of gene regulatory cues. Structure. 2006; 14:511–520. [PubMed: 16531235]

Hertzberg RP, Dervan PB. Cleavage of DNA with methidiumpropyl-EDTA-iron(II): reaction conditions and product analyses. Biochemistry. 1984; 23:3934–3945. [PubMed: 6435669]

Hohn M, Tang G, Goodyear G, Baldwin PR, Huang Z, Penczek PA, Yang C, Glaeser RM, Adams PD, Ludtke SJ. SPARX, a new environment for Cryo-EM image processing. J Struct Biol. 2007; 157:47–55. [PubMed: 16931051]

Jacobson RH, Ladurner AG, King DS, Tjian R. Structure and function of a human TAFII250 double bromodomain module. Science. 2000; 288:1422–1425. [PubMed: 10827952]

Juven-Gershon T, Cheng S, Kadonaga JT. Rational design of a super core promoter that enhances gene expression. Nat Methods. 2006; 3:917–922. [PubMed: 17124735]

Juven-Gershon T, Kadonaga JT. Regulation of gene expression via the core promoter and the basal transcriptional machinery. Dev Biol. 2010; 339:225–229. [PubMed: 19682982]

Kim JL, Nikolov DB, Burley SK. Co-crystal structure of TBP recognizing the minor groove of a TATA element. Nature. 1993a; 365:520–527. [PubMed: 8413605]

Kim Y, Geiger JH, Hahn S, Sigler PB. Crystal structure of a yeast TBP/TATA-box complex. Nature. 1993b; 365:512–520. [PubMed: 8413604]

Lander GC, Stagg SM, Voss NR, Cheng A, Fellmann D, Pulokas J, Yoshioka C, Irving C, Mulder A, Lau PW, et al. Appion: an integrated, database-driven pipeline to facilitate EM image processing. J Struct Biol. 2009; 166:95–102. [PubMed: 19263523]

Leschziner AE, Nogales E. The orthogonal tilt reconstruction method: an approach to generating single-class volumes with no missing cone for ab initio reconstruction of asymmetric particles. J Struct Biol. 2006; 153:284–299. [PubMed: 16431136]

Leschziner AE, Nogales E. Visualizing flexibility at molecular resolution: analysis of heterogeneity in single-particle electron microscopy reconstructions. Annu Rev Biophys Biomol Struct. 2007; 36:43–62. [PubMed: 17201674]

Leurent C, Sanders S, Ruhlmann C, Mallouh V, Weil PA, Kirschner DB, Tora L, Schultz P. Mapping histone fold TAFs within yeast TFIID. EMBO J. 2002; 21:3424–3433. [PubMed: 12093743]

Leurent C, Sanders SL, Demeny MA, Garbett KA, Ruhlmann C, Weil PA, Tora L, Schultz P. Mapping key functional sites within yeast TFIID. EMBO J. 2004; 23:719–727. [PubMed: 14765106]

Levine M. Paused RNA polymerase II as a developmental checkpoint. Cell. 2011; 145:502–511. [PubMed: 21565610]

Levine M, Tjian R. Transcription regulation and animal diversity. Nature. 2003; 424:147–151. [PubMed: 12853946]

Lieberman PM, Berk AJ. A mechanism for TAFs in transcriptional activation: activation domain enhancement of TFIID-TFIIA--promoter DNA complex formation. Genes Dev. 1994; 8:995–1006. [PubMed: 7926793]

Liu D, Ishima R, Tong KI, Bagby S, Kokubo T, Muhandiram DR, Kay LE, Nakatani Y, Ikura M. Solution structure of a TBP-TAF(II)230 complex: protein mimicry of the minor groove surface of the TATA box unwound by TBP. Cell. 1998; 94:573–583. [PubMed: 9741622]

Liu WL, Coleman RA, Grob P, King DS, Florens L, Washburn MP, Geles KG, Yang JL, Ramey V, Nogales E, et al. Structural changes in TAF4b-TFIID correlate with promoter selectivity. Mol Cell. 2008; 29:81–91. [PubMed: 18206971]

Liu WL, Coleman RA, Ma E, Grob P, Yang JL, Zhang Y, Dailey G, Nogales E, Tjian R. Structures of three distinct activator-TFIID complexes. Genes Dev. 2009; 23:1510–1521. [PubMed: 19571180]

Ludtke SJ, Baldwin PR, Chiu W. EMAN: semiautomated software for high-resolution single-particle reconstructions. J Struct Biol. 1999; 128:82–97. [PubMed: 10600563]

Mindell JA, Grigorieff N. Accurate determination of local defocus and specimen tilt in electron microscopy. J Struct Biol. 2003; 142:334–347. [PubMed: 12781660]

Nikolov DB, Chen H, Halay ED, Usheva AA, Hisatake K, Lee DK, Roeder RG, Burley SK. Crystal structure of a TFIIB-TBP-TATA-element ternary complex. Nature. 1995; 377:119–128. [PubMed: 7675079]

Ogura T, Iwasaki K, Sato C. Topology representing network enables highly accurate classification of protein images taken by cryo electron-microscope without masking. J Struct Biol. 2003; 143:185–200. [PubMed: 14572474]

Papai G, Tripathi MK, Ruhlmann C, Layer JH, Weil PA, Schultz P. TFIIA and the transactivator Rap1 cooperate to commit TFIID for transcription initiation. Nature. 2010; 465:956–960. [PubMed: 20559389]

Papai G, Tripathi MK, Ruhlmann C, Werten S, Crucifix C, Weil PA, Schultz P. Mapping the initiator binding Taf2 subunit in the structure of hydrated yeast TFIID. Structure. 2009; 17:363–373. [PubMed: 19278651]

Papai G, Weil PA, Schultz P. New insights into the function of transcription factor TFIID from recent structural studies. Curr Opin Genet Dev. 2011; 21:219–224. [PubMed: 21420851]

Papavassiliou AG. Chemical nucleases as probes for studying DNA-protein interactions. Biochem J. 1995; 305(Pt 2):345–357. [PubMed: 7832744]

Rhee HS, Pugh BF. Genome-wide structure and organization of eukaryotic pre-initiation complexes. Nature. 2012; 483:295–301. [PubMed: 22258509]

Sanders SL, Garbett KA, Weil PA. Molecular characterization of Saccharomyces cerevisiae TFIID. Mol Cell Biol. 2002; 22:6000–6013. [PubMed: 12138208]

Sawadogo M, Roeder RG. Interaction of a gene-specific transcription factor with the adenovirus major late promoter upstream of the TATA box region. Cell. 1985; 43:165–175. [PubMed: 4075392]

Sorzano CO, Marabini R, Velazquez-Muriel J, Bilbao-Castro JR, Scheres SH, Carazo JM, Pascual-Montano A. XMIPP: a new generation of an open-source image processing package for electron microscopy. J Struct Biol. 2004; 148:194–204. [PubMed: 15477099]

Suloway C, Pulokas J, Fellmann D, Cheng A, Guerra F, Quispe J, Stagg S, Potter CS, Carragher B. Automated molecular microscopy: the new Leginon system. J Struct Biol. 2005; 151:41–60. [PubMed: 15890530]

Sun X, Ma D, Sheldon M, Yeung K, Reinberg D. Reconstitution of human TFIIA activity from recombinant polypeptides: a role in TFIID-mediated transcription. Genes Dev. 1994; 8:2336–2348. [PubMed: 7958900]

Tang G, Peng L, Baldwin PR, Mann DS, Jiang W, Rees I, Ludtke SJ. EMAN2: an extensible image processing suite for electron microscopy. J Struct Biol. 2007; 157:38–46. [PubMed: 16859925]

Theisen JW, Lim CY, Kadonaga JT. Three key subregions contribute to the function of the downstream RNA polymerase II core promoter. Mol Cell Biol. 2010; 30:3471–3479. [PubMed: 20457814]

Thomas MC, Chiang CM. The general transcription machinery and general cofactors. Crit Rev Biochem Mol Biol. 2006; 41:105–178. [PubMed: 16858867]

Uchida K, Pyle AM, Morii T, Barton JK. High resolution footprinting of EcoRI and distamycin with Rh(phi)2(bpy)3+, a new photofootprinting reagent. Nucleic Acids Res. 1989; 17:10259–10279. [PubMed: 2602152]

Van Dyke MW, Hertzberg RP, Dervan PB. Map of distamycin, netropsin, and actinomycin binding sites on heterogeneous DNA: DNA cleavage-inhibition patterns with methidiumpropyl-EDTA.Fe(II). Proc Natl Acad Sci U S A. 1982; 79:5470–5474. [PubMed: 6291045]

Van Dyke MW, Roeder RG, Sawadogo M. Physical analysis of transcription preinitiation complex assembly on a class II gene promoter. Science. 1988; 241:1335–1338. [PubMed: 3413495]

van Heel M, Harauz G, Orlova EV, Schmidt R, Schatz M. A new generation of the IMAGIC image processing system. J Struct Biol. 1996; 116:17–24. [PubMed: 8742718]

Werten S, Mitschler A, Romier C, Gangloff YG, Thuault S, Davidson I, Moras D. Crystal structure of a subcomplex of human transcription factor TFIID formed by TATA binding protein-associated factors hTAF4 (hTAF(II)135) and hTAF12 (hTAF(II)20). J Biol Chem. 2002; 277:45502–45509. [PubMed: 12237304]

Wright KJ, Marr MT 2nd, Tjian R. TAF4 nucleates a core subcomplex of TFIID and mediates activated transcription from a TATA-less promoter. Proc Natl Acad Sci U S A. 2006; 103:12347–12352. [PubMed: 16895980]

Xie X, Kokubo T, Cohen SL, Mirza UA, Hoffmann A, Chait BT, Roeder RG, Nakatani Y, Burley SK. Structural similarity between TAFs and the heterotetrameric core of the histone octamer. Nature. 1996; 380:316–322. [PubMed: 8598927]

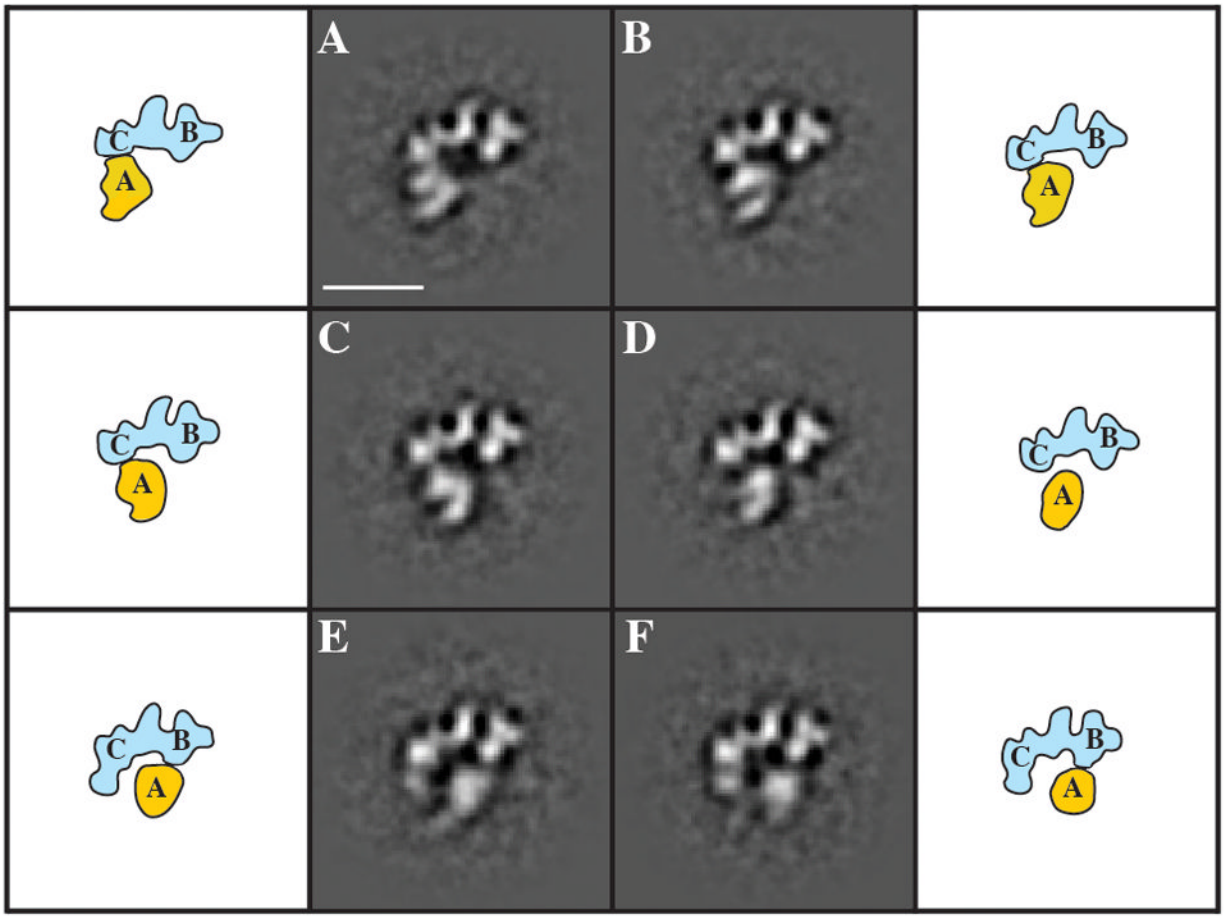

Figure 1. Lobe A exists in a range of positions relative to a stable BC core within the purified TFIID complex

2D reference-free cryo-EM class averages of TFIID shown alongside contour models to indicate lobe positions within each average. Lobe A is colored yellow whereas the stable BC core is colored blue. Scale bar in (A) is 200 Å. See also Figure S1 & Supplementary Movie 1.

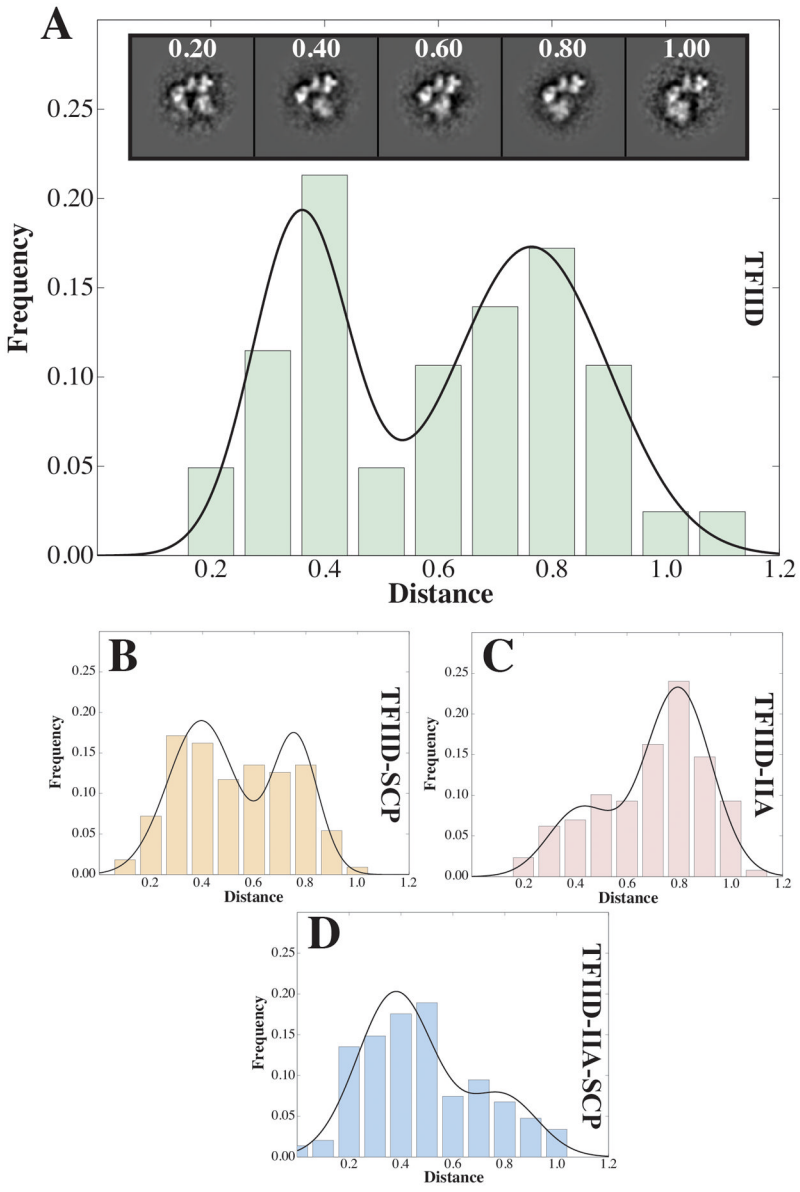

Figure 2. TFIID's conformational landscape changes in response to TFIIA and SCP DNA

Distribution of lobe A positions relative to the stable BC core for TFIID (A), TFIID-SCP (B), TFIID-TFIIA (C), and TFIID-TFIIA-SCP samples (D). Inset within (A): Class averages corresponding to specific lobe A measurements from the TFIID sample. See also Figure S1.

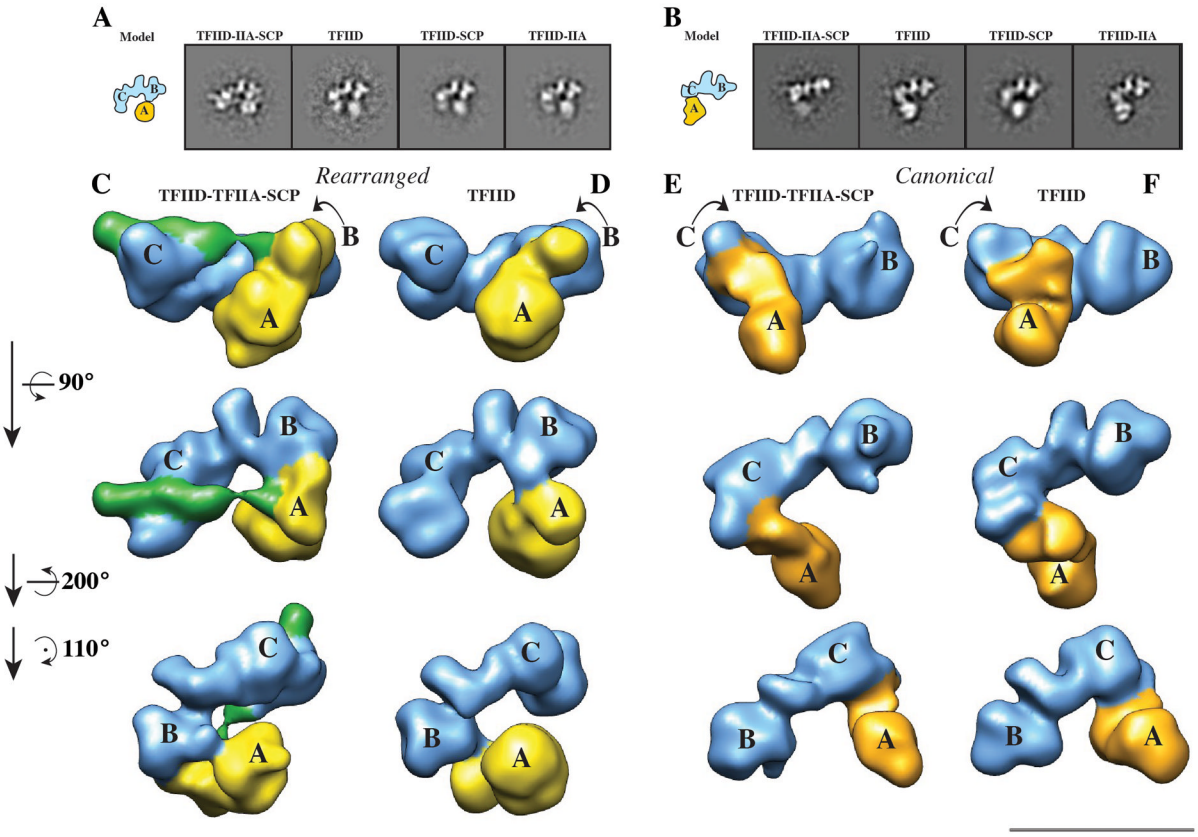

Figure 3. TFIIA-mediated binding of SCP DNA to the rearranged state of TFIID

Cryo-EM 2D reference-free class averages of the rearranged conformation (A) and the canonical conformation (B) shown alongside contour models. 3D reconstructions of the rearranged conformation for TFIID-TFIIA-SCP at 32 Å (C) and TFIID at 35 Å (D), where the density attributed to DNA in (C) is shown in green. 3D reconstructions of the canonical conformation for TFIID-TFIIA-SCP at 32 Å (E) and TFIID at 35 Å (F). The stable BC core is colored blue for each model. Lobe A is colored yellow for (C) and (D) and orange for (E) and (F). Scale bar is 200Å. See also Figures S2 & S3.

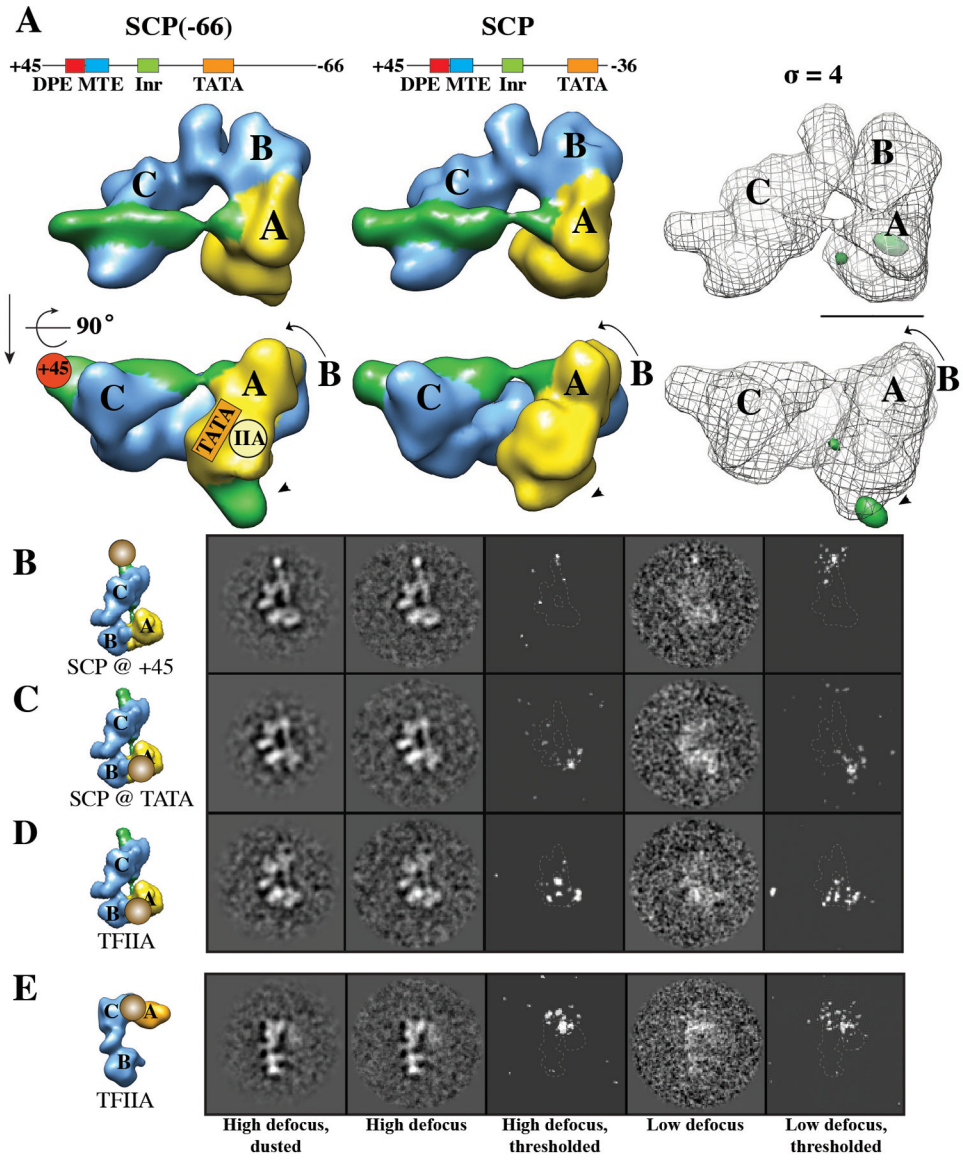

Figure 4. Organization of promoter DNA and TFIIA within the TFIID-IIA-SCP complex

(A) Cryo-EM reconstruction of TFIID-IIA-SCP(−66) at 35 Å (left column) aligned with the cryo-EM reconstruction of TFIID-IIA-SCP (center) and their difference map (right). DNA density is colored in green, whereas lobe A and the BC core are colored in yellow and blue, respectively. Scale bar is 100 Å. 2D reference-free class averages for the rearranged TFIID-TFIIA-SCP complex with Nanogold labels on SCP DNA at +45 (B), SCP DNA at TATA (C), and TFIIA (D). (E) 2D reference-free class average for the canonical state of TFIID-TFIIA-SCP containing Nanogold labeled on TFIIA. 3D models are shown alongside high defocus averages (density threshold at σ = 3.5) with a gold sphere marking the localization of Nanogold for each experiment. See Extended Experimental Procedures for a detailed discussion of generating low defocus class averages. Summary of gold labeling results for (B – D) are shown in (A), 2nd row.

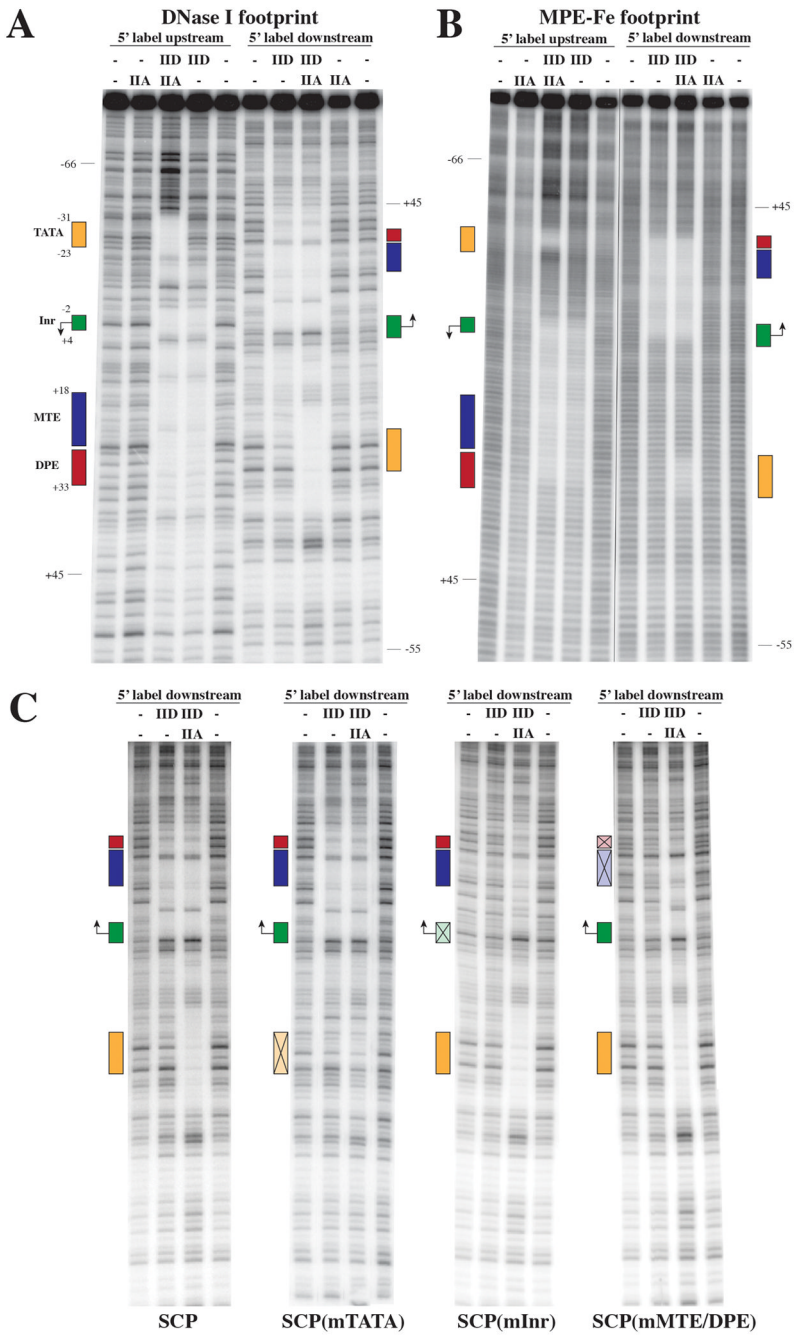

Figure 5. Core promoter architecture dictates TFIIA-dependent and TFIIA- independent interactions of TFIID with core promoter DNA

DNase I (A) and MPE-Fe (B) footprinting of TFIID-SCP and TFIID-TFIIA-SCP. (C) DNase I footprinting on 'wild type' and 'mutant' SCP DNA sequences. 5′ labeled downstream probes were analyzed for DNase I protection in the presence or absence of TFIIA for wild type, mutant TATA (mTATA), Inr (mInr), and MTE/DPE (mMTE/DPE). See also Figures S4 & S6.

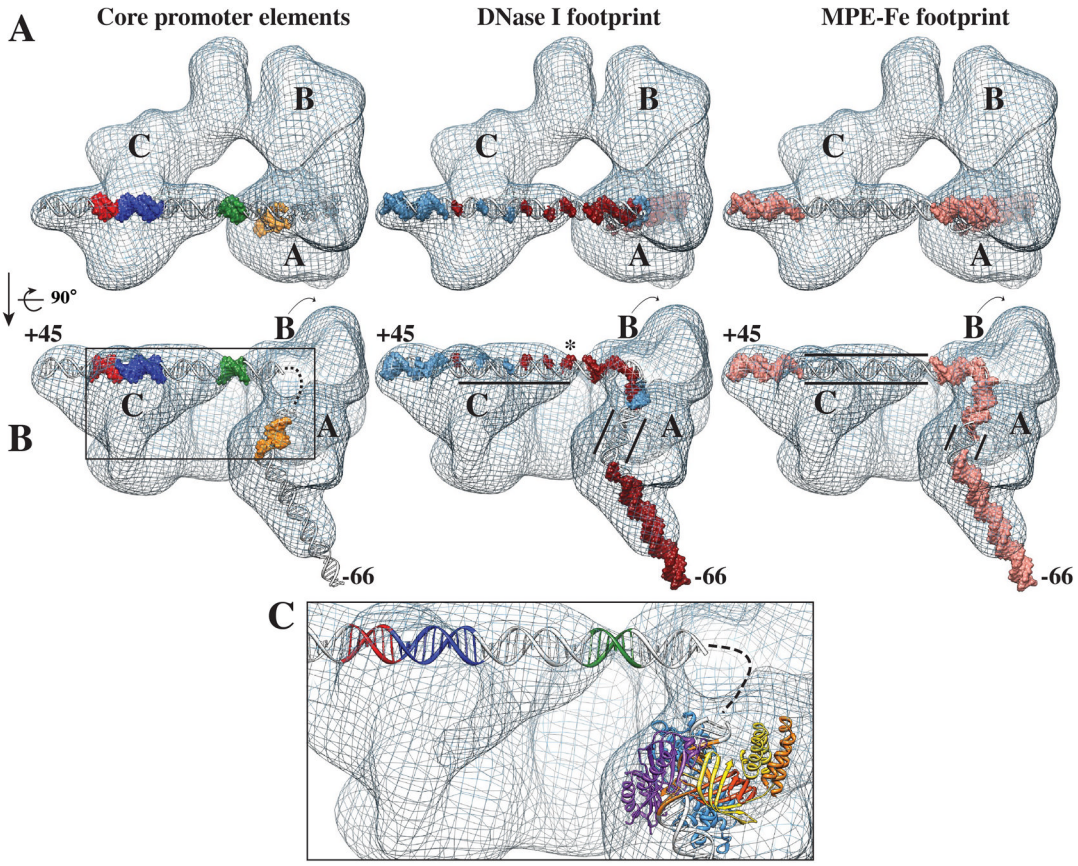

Figure 6. Structural description of the rearranged TFIID-IIA-SCP complex relative to the TSS

Promoter DNA for SCP(−66) docked into the TFIID-TFIIA-SCP(−66) map (shown in mesh). (A) & (B): DNA models were taken from Figure 5C for sequences from −66 to +45. Asterisk (*) in (B) indicates DNase I hypersensitive site at +3. Black lines in (B) indicate regions of continuous protection along SCP helix. (C) The proposed location of the crystal structures of TBP-TFIIA-TFIIB on TATA box DNA is in close proximity to Inr (PDB accession codes 1VOL and 1NVP). The unresolved DNA path between Inr and TATA is indicated by a dotted line. See also Supplementary Movie 2.

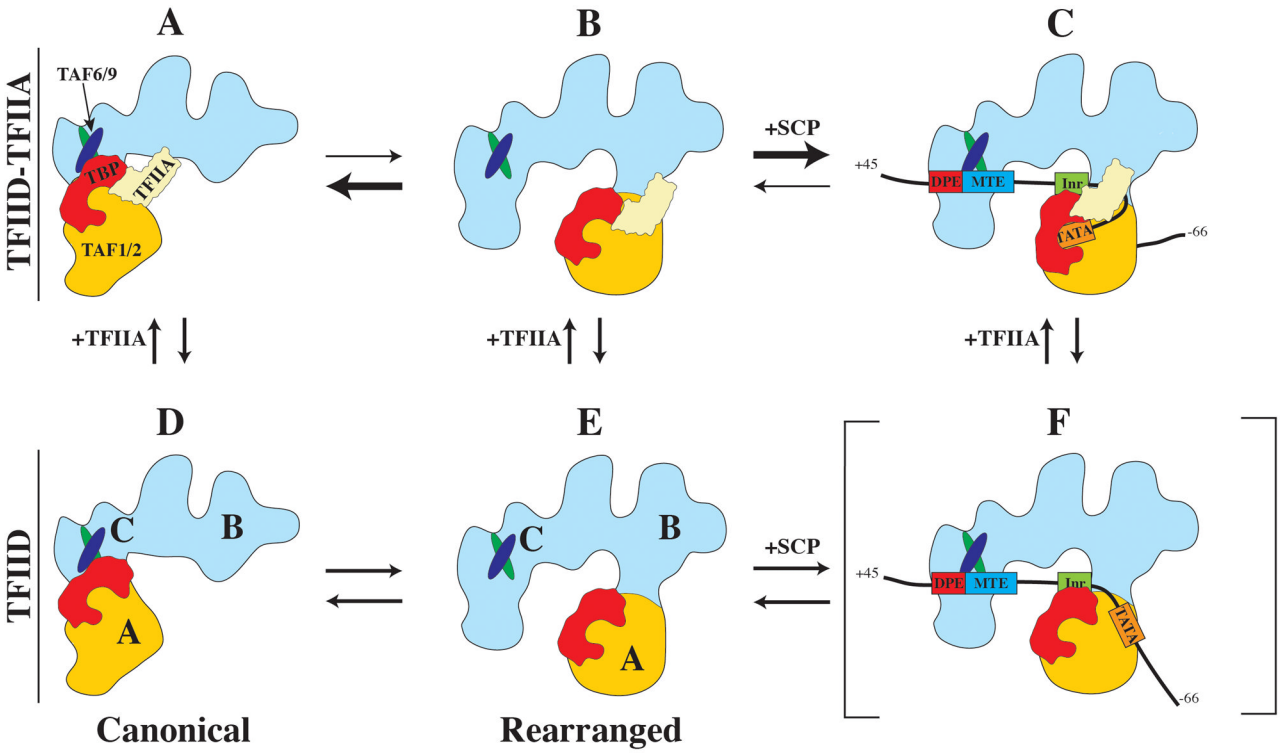

Figure 7. Model of TFIID's interaction with core promoter DNA in a conformation- and TFIIA-dependent fashion

Top row (A – C) describes conformations adopted by TFIID-TFIIA, while bottom row (D – F) describes TFIID alone. (A & B): TFIIA stabilizes TFIID in the canonical conformation. The addition of SCP DNA stabilizes the rearranged conformation for the ternary complex TFIID-TFIIA-SCP (C). In contrast to TFIID-TFIIA (A & B), TFIID adopts a conformational landscape that populates canonical and rearranged states equally (D & E). Upon addition, SCP DNA is bound by TFIID in the rearranged conformation (F). Brackets ([ ]) denote that (F) was observed only through biochemical footprinting.